ISCI, Volume *22*

Supplemental Information

cAMP-EPAC-Dependent Regulation of Gephyrin Phosphorylation and $GABA_AR$ Trapping at Inhibitory Synapses

Fumihiro Niwa, Angela Patrizio, Antoine Triller, and Christian G. Specht

Transparent Methods

Expression constructs

The coding sequence (cds) of Dendra2 (Clontech 632546) was inserted 3' of the signal peptide (SP) into the full-length cds of mouse $GABA_AR\gamma2$ (UniProt P22723-1, isoform 2L) in the lentivirus vector FUGW (Lois et al., 2002), to generate the replicon FU-Dendra2-$GABA_AR\gamma2$. The lentivirus constructs FU-Dendra2-GlyRα1 and FU-Dendra2-GlyRα3L (long isoform) were described previously (Patrizio et al., 2017). A short isoform lacking the residues T^{325}EAFALEKFYRFSDM^{339} of the ICD of GlyRα3 (Nikolic et al., 1998) was also constructed (FU-Dendra2-GlyRα3K). The phosphorylation variants FU-mEos4b-GlyRα3L^{S346A} and FU-mEos4b-GlyRα3L^{S346D} were obtained by site-directed mutagenesis from the mEos4b-version of the wild-type GlyRα3L construct (FU-mEos4b-GlyRα3L). Plasmid FU-mEos4b-gephyrin^{wt} (N-terminally tagged rat gephyrin, GenBank X66366, splice variant P1) and its PKA-insensitive variant FU-mEos4b-gephyrin^{PKA-} (S294A/S295A/S303A/S305A/S319A) were derived from an earlier construct (Patrizio et al., 2017). The putative PKA target sites were selected based on *in vivo* phosphorylation sites of gephyrin in the PhosphoSitePlus database (www.phosphosite.org; Hornbeck et al., 2015). Another gephyrin construct (mRFP-gephyrin; Calamai et al., 2009) was used for co-transfection together with N- and C-terminal fusion constructs of mEos4b with the cds of mouse EPAC2 (RapGef4, Source BioScience clone IRCLp5011D1135D, IMAGE clone ID IMAGE:40141811) in the FUGW vector.

Lentivirus production

Lentiviruses were produced as described previously (Grünewald et al., 2018). Briefly, HEK-293 cells were co-transfected with replicon DNA together with the two packaging plasmids pCMVR8.74 and pMD2.G (Addgene, plasmids #22036 and #12259) using lipofectamine 2000 (Thermo Fisher Scientific). Cells were kept in Neurobasal medium containing GlutaMAX and B27 at 32°C / 5% CO_2 for 24 h, at which time the medium was replaced. The lentivirus-containing medium was collected at 48-55 h after transfection, filtered with a pore size of 0.45 μm, and stored at -80°C.

Primary neuron cultures

Animals were treated in accordance with the guidelines of the French Ministry of Agriculture and the Direction Départementale des Services Vétérinaires de Paris (Ecole Normale Supérieure, Animalerie des Rogeurs, license B 75-05-20). Dissociated cultures of spinal cord neurons were prepared from Sprague Dawley rat embryos at developmental stage E14 and from mouse embryos at E13 as described previously (Specht et al., 2013), using heterozygous knock-in animals expressing mRFP-tagged gephyrin (Machado et al., 2011) in the C57BL/6J genomic background. Neurons were plated at a density of $1.6 \times 10^4/cm^2$ on 18 mm coverslips in Neurobasal medium containing GlutaMAX (Thermo Fisher), B27 (Thermo Fisher) and antibiotics. At day *in vitro* (DIV) 7 half of the medium was replaced with BrainPhys neuronal medium (STEMCELL Technologies), and thereafter twice a week. Spinal cord neurons were infected at DIV1-7 if required, and used for experiments at DIV14-20.

Organotypic slice cultures were prepared as previously described (Cantaut-Belarif et al., 2017). Spinal cords from mRFP-gephyrin KI animals at postnatal day P3-P7 were sliced using a McIllwain tissue chopper. Slices of 200 μm thickness were placed on Millicell CM inserts (Millipore) and cultured with MEM medium supplemented with 20% horse serum, 5% HBSS, GlutaMAX, 8 mM D-glucose, 20 mM HEPES and antibiotics. The medium was changed every 3 days and slice cultures were used for experiments up to DIV21.

Pharmacology for immunocytochemistry

Forskolin (Tocris) was dissolved in ethanol at a concentration of 10 mM, and used at a final concentration of 20 μM in culture medium for 30 min unless otherwise stated. In most experiments with forskolin, we used 0.2% ethanol as control condition (vehicle) except for the data shown in figures 2AB, 4AB, S1DE, S4 and S5. In these experiments, no ethanol was added in the control. The PKA antagonist H-89 (Sigma) was used at a final concentration of 2.5 μM. For the activation of EPAC, the cAMP analog 007-AM (8-(4-chloro-phenylthio)-2'-O-methyladenosine-3',5'-cyclic monophosphate acetoxymethyl ester; Tocris) was dissolved in DMSO at 5 mM and applied at a final concentration of 3 μM; the appropriate concentration of DMSO (0.06%) was added in the control condition of the experiments with 007. For immunocytochemistry, PP1/PP2a were blocked with 40 nM okadaic acid for 15 min prior to the treatment with Forskolin and H-89 for an additional 30 min (in the presence of okadaic acid). For details about the application of forskolin and 007-AM in the QD-SPT recordings see below.

Western blotting

Dissociated spinal cord neurons cultured in 6 well plates and infected with mEos4b-gephyrin lentivirus were treated at DIV14 with 20 μM forskolin or vehicle for 30 min (2 wells per condition), and collected on ice with buffer containing 50 mM Tris pH 7.5, 150 mM NaCl, 1% Nonidet P40 and 0.25% SDS, as well as protease inhibitors (complete EDTA-free, Roche) and phosphatase inhibitors (1 mM sodium orthovanadate, 1 mM sodium fluoride, 1 mM sodium molybdate, 4 mM sodium tartrate, 100 nM fenvalerate and 250 nM okadaic acid). Samples were loaded in reducing sample buffer and separated by SDS-PAGE, blotted onto PVDF membranes (Millipore), and labelled with mouse monoclonal anti-gephyrin antibody mAb7a (147 011, Synaptic Systems; Kuhse et al., 2012) and HRP-coupled secondary antibody. Antigens were detected by chemiluminescence and quantified with ImageJ. Membranes were stripped in buffer containing β-mercaptoethanol and SDS at 50ºC for 30 min and then re-labelled with anti-gephyrin antibody 3B11 (Synaptic Systems 147 111; Smolinsky et al., 2008).

For quantification, we analysed two sets of samples for each experiments: non-infected neurons and infected neurons, with or without forskolin treatment. The bands corresponding to endogenous gephyrin and recombinant mEos4b-gephyrin were quantified (i.e. 3 pairs of bands for each membrane). The experiment was repeated three times and the statistical analysis was done on the pooled data (i.e. n = 3 x 3 = 9 data pairs).

Immunolabelling

Immunolabelling was done as described by Patrizio et al. (2017). Fixed neurons were permeabilised in PBS with 0.1% Triton X100, blocked in PBS containing 2.5% BSA, and labelled with primary antibodies (rabbit anti-GlyRα1, custom made; mouse anti-gephyrin mAb7a, Synaptic Systems 147 011; rat anti-gephyrin mAb7a, Synaptic Systems 147 208; mouse anti-gephyrin 3B11, Synaptic Systems 147 111; mouse anti-$GABA_AR\beta3$, clone N87/25, NeuroMab 75-149; rabbit anti-Epac1, Abcam ab21236; rabbit anti-Epac2, Abcam ab21238). Primary antibodies were generally applied for 1 hour at a dilution of 1:500 with the exception of the EPAC antibodies (used at 1:200, 5 μg/ml), followed by secondary goat antibodies (Alexa Fluor 488 conjugated anti-mouse IgG, Cy3 anti-rabbit IgG, Alexa Fluor 647 anti-rat, Alexa Fluor 647 anti-mouse).

Live surface labeling of GlyRα1 was done as follows. Neurons were treated with 20 μM forskolin or vehicle (ethanol) for 15 min in culture medium at 37°C. Then, rabbit anti-GlyRα1 antibody was added at a 1:100 dilution for another 15 min. After fixation and blocking, GlyRs were labelled using secondary Alexa Fluor 488 conjugated anti-rabbit IgG.

Fluorescence image acquisition and analysis

Images of dissociated cultured neurons were acquired on an inverted Nikon Eclipse Ti microscope with a 100x oil-immersion objective (NA 1.49), using an Andor iXon EMCCD camera (16-bit, image pixel size: 160 nm, or 107 nm with an additional 1.5x lens in the emission path) and NIS-Elements software (Nikon). Specific emission filters were chosen for the detection of the different fluorophores: 525/30 for Alexa Fluor 488, unconverted Dendra2 and mEos4b, 607/36 for mRFP and Cy3, and 684/24 for Alexa Fluor 647. Confocal imaging of organotypic slices was done on an SP8 confocal microscope (Leica Microsystems). Nine consecutive single plane images were taken from the dorsal edge of the spinal cord slice towards the ventral region.

Images were always acquired with the same excitation intensity and exposure time in each channel for a given experiment to ensure comparability between experimental conditions. Quantitation was performed using a lab-made programme (ImAnalysis; Hennekinne et al., 2013) in Matlab (MathWorks). Binary masks of synaptic clusters of at least 3 pixels were created by image segmentation with multidimensional image analysis (MIA, Racine et al., 2007; or Spot Detector in Icy, de Chaumont et al., 2012, http://icy.bioimageanalysis.org/). Generally, the gephyrin image was used to generate the binary masks (mRFP-gephyrin in Fig. 2C-E, mEos4b in Fig. 4A-C and S1DE, 3B11 in Fig. 4G), with the exception of the data in figures 1, 2AB, 4E, S4 and S5, where the GlyR images were used to make the mask. For each cluster, the integrated fluorescence intensity was measured in each channel. In some experiments, data were background corrected using readings of diffuse fluorescence intensity in dendrites (Fig. 2AB, 4AB, S1, S4, S5).

Single molecule localisation microscopy (SMLM)

SMLM imaging was done as described elsewhere (Izeddin et al., 2011). Neurons expressing mEos4b-gephyrin were fixed and imaged in PBS in an open chamber. PALM movies of 10000 frames were recorded at 20 Hz with inclined 561 nm laser illumination (output power 40% of 500 mW, emission filter 607/36). mEos4b was photoconverted by 0.5 ms pulsed 405 nm laser illumination with a fixed intensity profile (output power during frames 1-1000 at 2%, 1000-5000 3%, 5000-10000 5% of a 120 mW laser). The focal plane was maintained using a Nikon perfect focus system. For STORM imaging, cultures were immunolabelled with mAb7a and Alexa Fluor 647 antibodies and imaged in STORM buffer composed of 10% glucose, 50 μM β-mercaptoethylamine, 0.5 mg/ml glucose oxidase, and 54 μg/ml catalase in PBS (pH 7.4). Movies of 10000 frames were acquired at 20 Hz with inclined 633 nm laser illumination (output power 80% of 800 mW, emission filter 684/24) and low intensity pulsed photoactivation at 405 nm (output power during frames 1-1000 at 0%, 1000-5000 20%, 5000-10000 50%).

Single fluorophores where detected by Gaussian fitting. The resulting pointillist images were corrected for drifts in the x/y plane using several dense clusters of detections in the images themselves as reference. Quantification of clusters of gephyrin in the pointillist images was done using a lab-made software in Matlab (CountMol; Patrizio et al., 2017). Synaptic clusters were detected by setting a lower threshold for cluster size (minimum length PALM: 100 nm; STORM: 100 nm), as well as the minimum number of detections (PALM: 200 detections; STORM: 50 detections).

Single-particle tracking (SPT)

The diffusion of Dendra2-tagged receptors expressed in spinal cord neurons was analysed by single-particle tracking (SPT) using quantum dots (QDs) as described before (Bannai et al., 2006; Patrizio et al., 2017). Cells were labelled with rabbit Dendra2 antibody (Antibodies-online ABIN361314) and anti-rabbit $F(ab')_2$ coupled QDs emitting at 605 nm, and imaged for up to 30 min in MEM based imaging buffer supplemented with 20 mM HEPES, 2 mM glutamine, 1 mM sodium pyruvate, 2% FBS and 33 mM glucose at 37°C. In the experiments shown in Fig. 6A, B, forskolin, 007-AM and vehicle (0.2% ethanol) were present during QD labelling and recording. For

the data in Fig. 6C, D, forskolin was pre-applied for 30 min, but absent during imaging. Synapses were stained with 1 μM FM4-64 dye applied in imaging buffer containing 40 mM KCl for 30 sec. Synaptic masks were created from these images using Spot Detector in Icy. QD trajectories (500 frames at 13 Hz) were analysed using homemade software in Matlab (Mathworks). Diffusion coefficients of QD-receptors were calculated by fitting of the first 5 points of the mean squared displacement (MSD) plot against time.

Statistical analysis

Immunocytochemical data were analysed with one-way ANOVA and Tukey's test for post hoc analysis, the Kruskal-Wallis (KW) test with Dunn's test for post hoc analysis, or with Welch's t-test. Western blot data were compared using a paired t-test that paired the corresponding conditions in each experiment. QD diffusion data were statistically compared using KW test and Dunn's post hoc test. SMLM data were analysed with Mann-Whitney's U-test (MW). A summary of the statistical information is provided in Table S1 (including tests, sample size, probabilities); Table S2 is a compilation of all the mean values and quartiles displayed in the figures.

References

Bannai, H., Levi, S., Schweizer, C., Dahan, M., and Triller, A. (2006). Imaging the lateral diffusion of membrane molecules with quantum dots. Nat Protoc *1*, 2628-2634.

Calamai, M., Specht, C.G., Heller, J., Alcor, D., Machado, P., Vannier, C., and Triller, A. (2009). Gephyrin oligomerization controls GlyR mobility and synaptic clustering. J Neurosci *29*, 7639-7648.

Cantaut-Belarif, Y., Antri, M., Pizzarelli, R., Colasse, S., Vaccari, I., Soares, S., Renner, M., Dallel, R., Triller, A., and Bessis, A. (2017). Microglia control the glycinergic but not the GABAergic synapses via prostaglandin E2 in the spinal cord. J Cell Biol *216*, 2979-2989.

de Chaumont, F., Dallongeville, S., Chenouard*, et al.* (2012). Icy: an open bioimage informatics platform for extended reproducible research. Nat Methods *9*, 690-696.

Grünewald, N., Jan, A., Salvatico, C., Kress, V., Renner, M., Triller, A., Specht, C.G., and Schwarz, G. (2018). Sequences flanking the gephyrin-binding site of GlyRbeta tune receptor stabilization at synapses. eNeuro *5*.

Hennekinne, L., Colasse, S., Triller, A., and Renner, M. (2013). Differential control of thrombospondin over synaptic glycine and AMPA receptors in spinal cord neurons. J Neurosci *33*, 11432-11439.

Hornbeck, P.V., Zhang, B., Murray, B., Kornhauser, J.M., Latham, V., and Skrzypek, E. (2015). PhosphoSitePlus, 2014: mutations, PTMs and recalibrations. Nucleic Acids Res *43*, D512-520.

Izeddin, I., Specht, C.G., Lelek, M., Darzacq, X., Triller, A., Zimmer, C., and Dahan, M. (2011). Super-resolution dynamic imaging of dendritic spines using a low-affinity photoconvertible actin probe. PLoS One *6*, e15611.

Kuhse, J., Kalbouneh, H., Schlicksupp, A., Mukusch, S., Nawrotzki, R., and Kirsch, J. (2012). Phosphorylation of gephyrin in hippocampal neurons by cyclin-dependent kinase CDK5 at Ser-270 is dependent on collybistin. J Biol Chem *287*, 30952-30966.

Lois, C., Hong, E.J., Pease, S., Brown, E.J., and Baltimore, D. (2002). Germline transmission and tissue-specific expression of transgenes delivered by lentiviral vectors. Science *295*, 868-872.

Machado, P., Rostaing, P., Guigonis, J.M., Renner, M., Dumoulin, A., Samson, M., Vannier, C., and Triller, A. (2011). Heat shock cognate protein 70 regulates gephyrin clustering. J Neurosci *31*, 3-14.

Nikolic, Z., Laube, B., Weber, R.G., Lichter, P., Kioschis, P., Poustka, A., Mulhardt, C., and Becker, C.M. (1998). The human glycine receptor subunit alpha3. Glra3 gene structure, chromosomal localization, and functional characterization of alternative transcripts. J Biol Chem *273*, 19708-19714.

Patrizio, A., Renner, M., Pizzarelli, R., Triller, A., and Specht, C.G. (2017). Alpha subunit-dependent glycine receptor clustering and regulation of synaptic receptor numbers. Sci Rep *7*, 10899.

Racine, V., Sachse, M., Salamero, J., Fraisier, V., Trubuil, A., and Sibarita, J.B. (2007). Visualization and quantification of vesicle trafficking on a three-dimensional cytoskeleton network in living cells. J Microsc *225*, 214-228.

Smolinsky, B., Eichler, S.A., Buchmeier, S., Meier, J.C., and Schwarz, G. (2008). Splice-specific functions of gephyrin in molybdenum cofactor biosynthesis. J Biol Chem *283*, 17370-17379.

Specht, C.G., Izeddin, I., Rodriguez, P.C., El Beheiry, M., Rostaing, P., Darzacq, X., Dahan, M., and Triller, A. (2013). Quantitative nanoscopy of inhibitory synapses: counting gephyrin molecules and receptor binding sites. Neuron *79*, 308-321.

Supplemental figures and tables

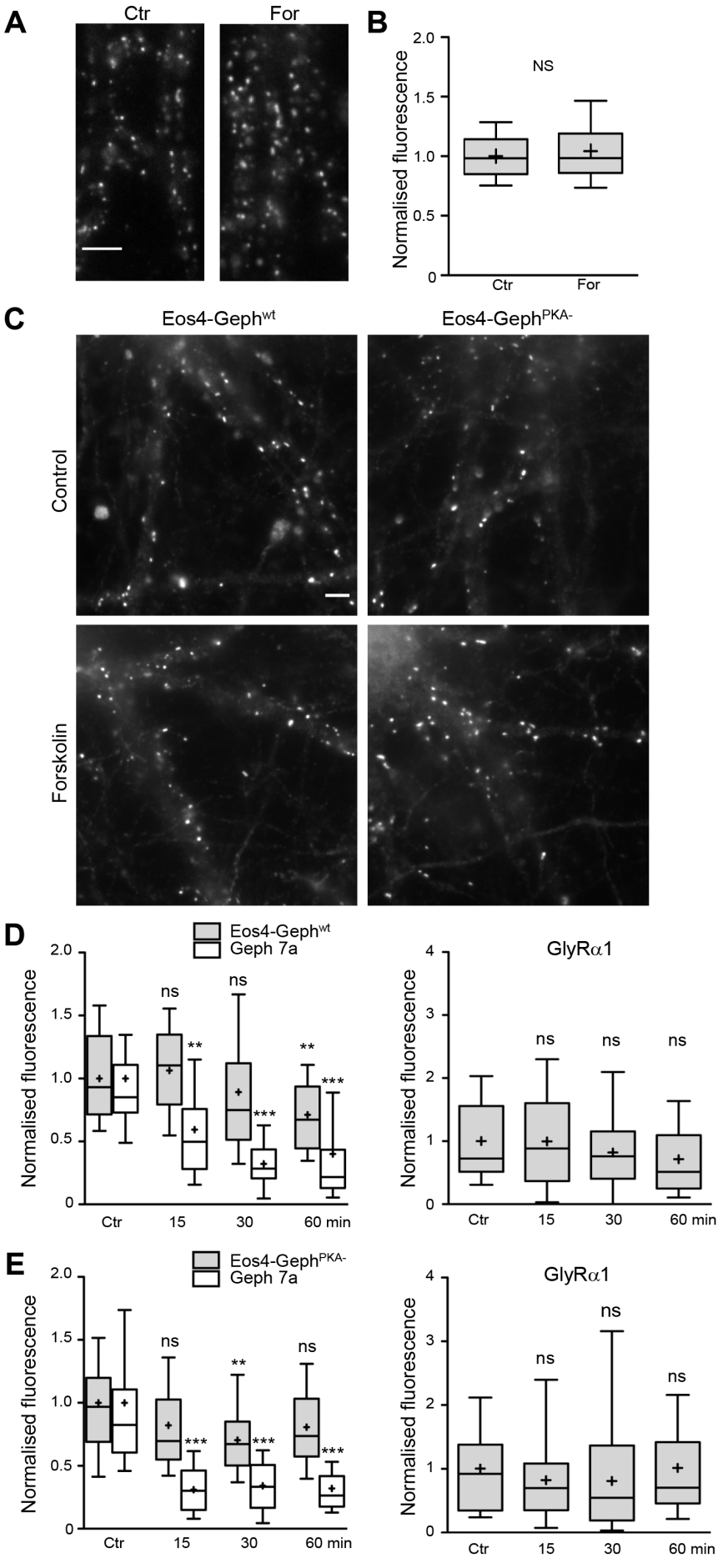

Figure S1. Effect of forskolin on GlyRα1 and gephyrin (related to Fig. 1).

(A) Immunocytochemistry of surface labelled GlyRα1 treated with or without forskolin. Scale: 5 µm. **(B)** Quantification of fluorescence intensity of surface GlyRα1 clusters (n_{Ctr} = 80, n_{For} = 80 cells from 2 experiments; p = 0.27, t-test). **(C)** Overview images of Eos4-Geph^{wt} and Eos4-Geph^{PKA-} expressing neurons with or without forskolin treatment, showing proximal dendrites crossing the whole image. Scale: 5 µm. **(D)** Eos4-Geph^{wt} and **(E)** Eos4-Geph^{PKA-} expressing neurons were treated with forskolin for 15, 30 or 60 min, or without forskolin (Ctr), fixed and labelled with anti-GlyRα1 and mAb7a antibodies. Both, neurons expressing Eos4-Geph^{wt} and Eos4-Geph^{PKA-} showed a significant reduction of gephyrin phosphorylation (mAb7a) in response to forskolin, whereas total mEos4-gephyrin levels and GlyRα1 labelling remained relatively stable. Data were normalised to the control condition in each channel for each construct and each experiment. Note that the left panels in (D, E) are the same data as those used to calculate the mAb7a/Eos4 ratios in Fig. 4B. Data are represented as 10%, 25%, 50%, 75% and 90% percentiles; the mean is indicated as a cross; **p < 0.01, ***p < 0.001, ANOVA.

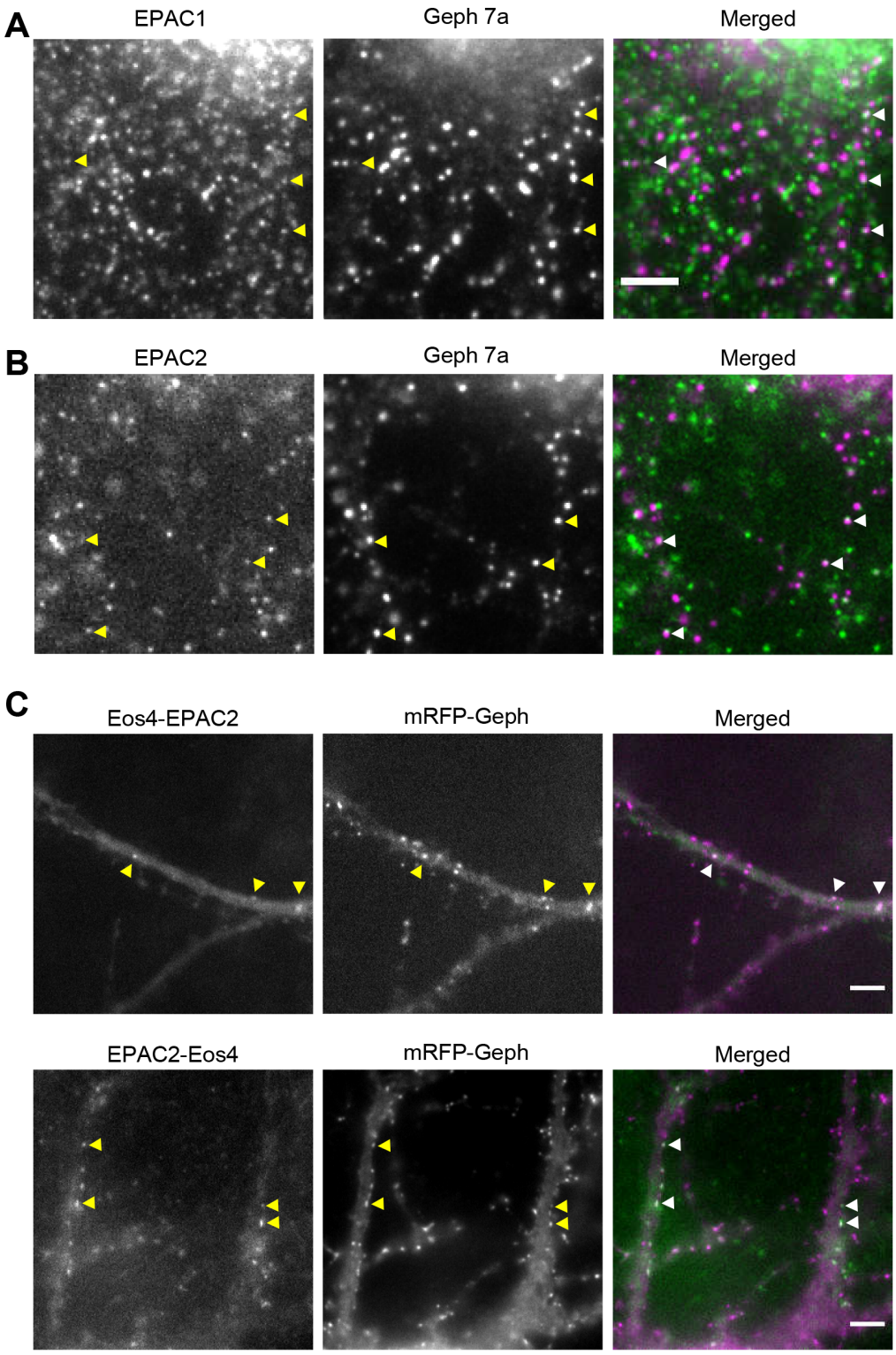

Figure S2. EPAC is present at inhibitory synapses in spinal cord neurons (related to Fig. 4). Cultured rat spinal cord neurons were immunolabelled with antibodies against EPAC1 **(A)** and EPAC2 **(B)**, as well as with the gephyrin antibody mAb7a. The partial co-localisation of the EPAC proteins (shown in green in the merged images) and the inhibitory synaptic gephyrin scaffold (red) is indicated by arrowheads. **(C)** Spinal cord neurons co-transfected with mRFP-gephyrin (magenta) and N- or C-terminally tagged EPAC2 (constructs FU-mEos4b-EPAC2 and FU-EPAC2-mEos4b, green). EPAC2 co-localises with a sub-population of mRFP-gephyrin clusters (arrowheads) at inhibitory synapses. Scale: 5 µm.

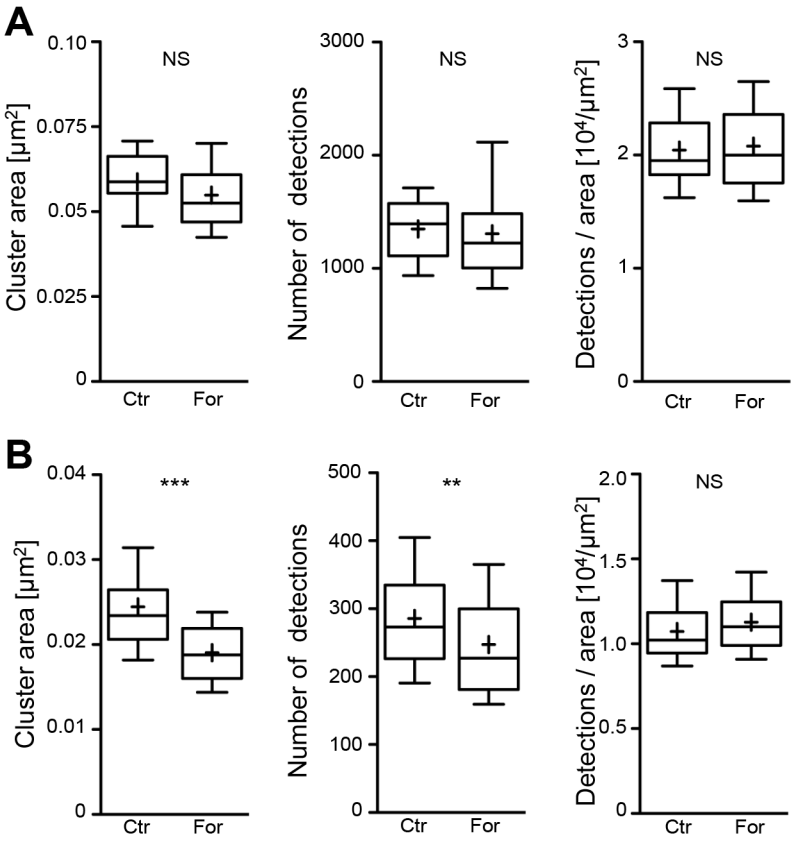

Figure S3. Cell by cell analysis of SMLM data of synaptic gephyrin clusters (related to Fig. 5). **(A)** Quantification of synaptic cluster areas, detection numbers, and detection densities by PALM imaging with mEos4b-gephyrin (n_{Ctr} = 32, for n_{For} = 32 cells from 3 independent experiments; area p = 0.65, detections p = 0.14, detection/area p = 0.73, t-test). **(B)** The quantification of cluster area and number of mAb7a (Alexa 647) detections in dSTORM images shows a correlated decrease in forskolin treated neurons compared to control (n_{Ctr} = 70, for n_{For} = 66 from 3 independent experiments; area ***p < 0.0001, detections **p < 0.01, detection/area p = 0.09, t-test). Cell by cell analysis did not reveal any significant differences in the detection densities of total (Eos4, **A**) or pS270-gephyrin (mAb7a, **B**), in contrast to the synapse by synapse analysis of the same dataset (see Fig. 5).

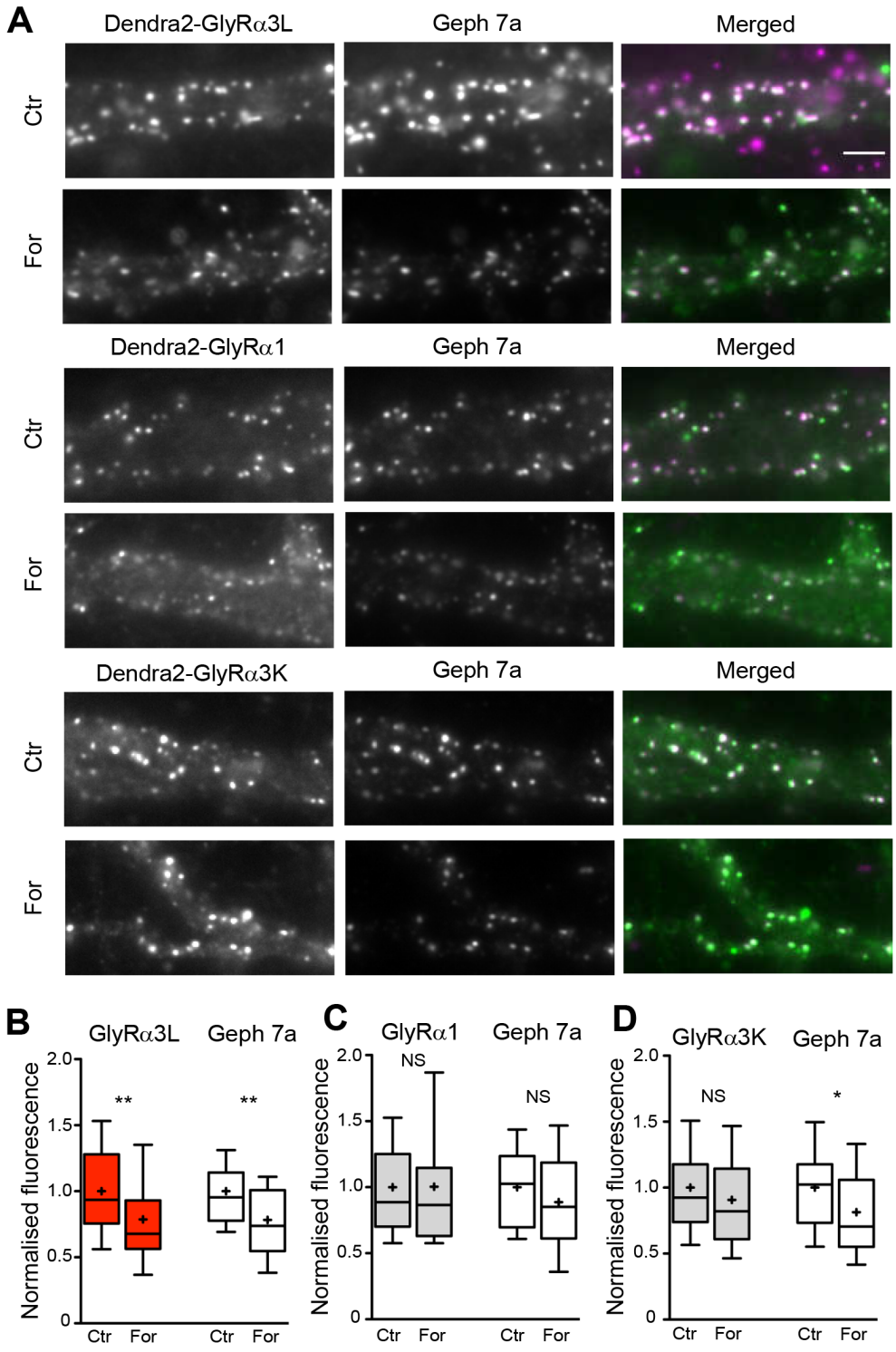

Figure S4. Forskolin specifically alters GlyRα3L levels at synapses (related to Fig. 6).
(A) Lentivirus-infected rat spinal cord neurons expressing Dendra2-GlyRα1, α3K, or α3L (green in merged image) were treated with or without forskolin, fixed, and labelled with mAb7a antibody (magenta in merged image). Scale: 5 µm. **(B)** Dendra2-GlyRα3L fluorescence levels at synapses were decreased by 22 ± 5% following 30 min of treatment with forskolin (n_{Ctr} = 70, n_{For} = 61 cells from 3 experiments). **(C)** Dendra2-GlyRα1 fluorescence at synapses was not affected by forskolin (n_{Ctr} = 53, n_{For} = 32). **(D)** Forskolin did not alter the levels of synaptic Dendra2-GlyRα3K (n_{Ctr} = 68, n_{For} = 69). Gephyrin labelling with the phospho-specific antibody mAb7a at Dendra2 puncta was consistently reduced in all experiments (B-D). Data are represented as 10%, 25%, 50%, 75% and 90% percentiles and the mean (as cross); *$p < 0.05$, **$p < 0.01$, ANOVA.

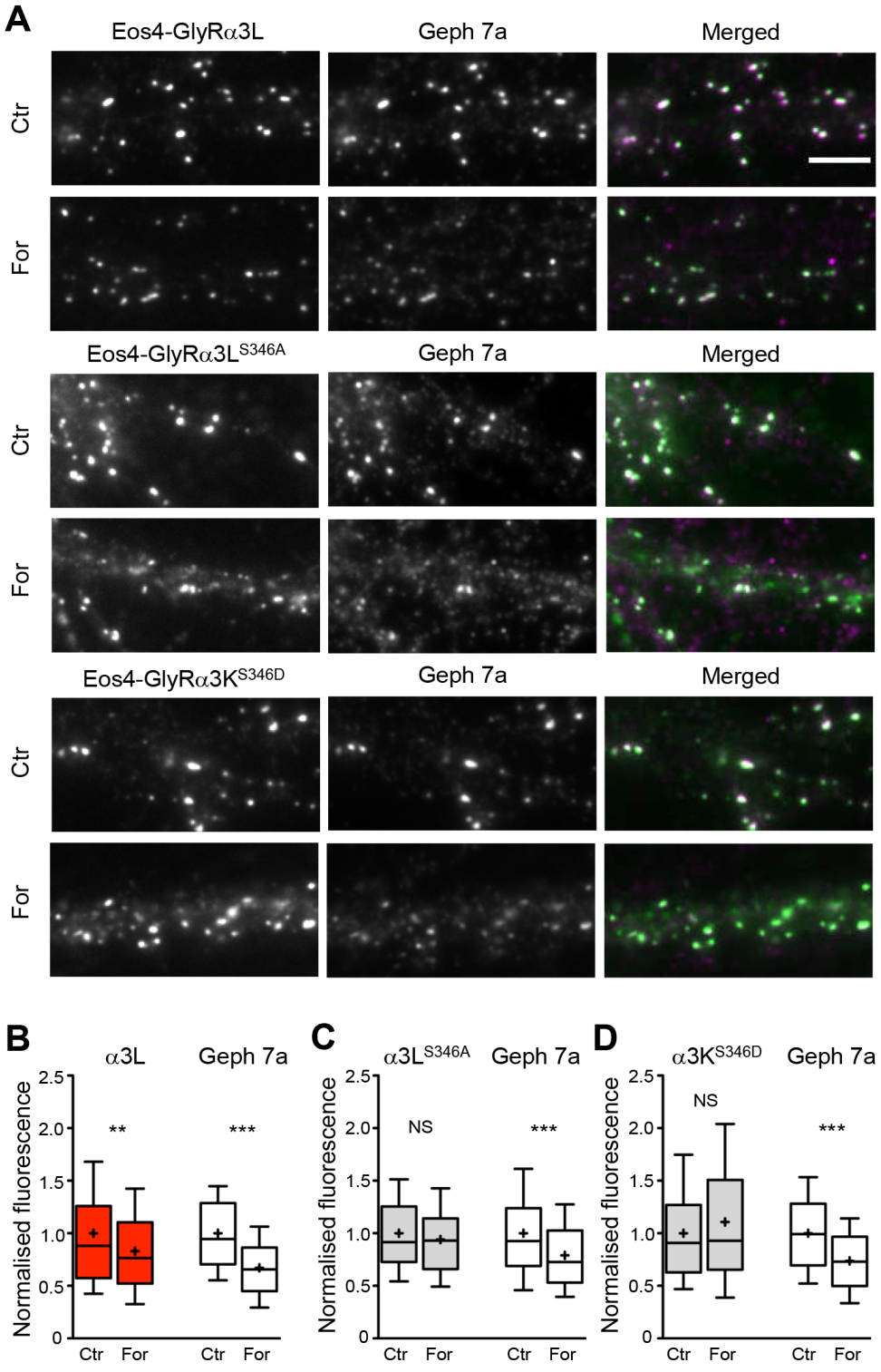

Figure S5. GlyRα3L clustering is regulated by S346 phosphorylation (related to Fig. 6).
(A) Lentivirus-infected rat spinal cord neurons expressing wildtype Eos4-GlyRα3L or the phosphorylation mutants Eos4-GlyRα3L^{S346A} or Eos4-GlyRα3L^{S346D} (green) were treated with or without forskolin, fixed, and labelled with mAb7a antibody (magenta). Scale: 5 µm. **(B-D)** Gephyrin labelling with the phospho-specific antibody mAb7a was consistently reduced at synapses by 30 min of treatment with forskolin, as was Eos4-GlyRα3L fluorescence (**B**, n_{Ctr} = 146, n_{For} = 159 cells from 3 experiments). In contrast, Eos4-GlyRα3L^{S346A} (**C**, n_{Ctr} = 159, n_{For} = 146) and Eos4-GlyRα3L^{S346D} levels (**D**, n_{Ctr} = 164, n_{For} = 141) at synapses were not affected by forskolin treatment. Data are shown as percentiles of the population (10%, 25%, 50%, 75%, 90%) and the mean (cross); **p < 0.01, ***p < 0.001, ANOVA.

Table S1. Statistical evaluation of the data including applied tests, sample size, and p-values (related to Figures 1-6).

Figure Number	Used Statistics	Type of sample	Type of analysis	Sample number (n)	P value
Fig. 1B	1 way anova with Tukey's Multiple comparison test as post hoc test	Mean intensity of each cluster in a cell	Cell by cell	$n_{Ctr} = 86$, $n_{For} = 79$	P<0.0001
Fig. 1C	1 way anova with Tukey's Multiple comparison test as post hoc test	Ratio of receptor / gephyrin in each cluster	cluster by cluster	$n_{Ctr} = 14218$, $n_{For} = 12334$	P<0.0001
Fig. 2B	1 way anova with Tukey's Multiple comparison test as post hoc test	Mean intensity of each cluster in a cell	Cell by cell	GlyRa1: $n_{Ctr} = 149$, $n_{For} = 144$; mAb7a: $n_{Ctr} = 60$, $n_{For} = 56$; 3B11: $n_{Ctr} = 89$, $n_{For} = 88$	P<0.0001
Fig. 2D	1 way anova with Tukey's Multiple comparison test as post hoc test	Mean intensity of each cluster in a cell	Cell by cell	$n_{Ctr} = 39$, $n_{For} = 40$	P=0.5651
Fig. 2E Control vs forskolin	Welch's t test	Mean intensity of each cluster in an image	image by image	$n_{Ctr} = 44$, $n_{For} = 57$	P<0.0001
Fig. 2E comparison of different timepoint	1 way anova with Tukey's Multiple comparison test as post hoc test	Mean intensity of each cluster in an image	image by image	$n_{Ctr2-3} = 14$, $n_{Ctr4-5} = 14$, $n_{Ctr6-7} = 10$, $n_{Ctr8-9} = 6$, $n_{For2-3} = 16$, $n_{For4-5} = 16$, $n_{For6-7} = 13$, $n_{For8-9} = 12$,	Ctr P=0.1255 , For P=0.0721
Fig. 3B	Paired t test	Mean intensity of each band in each condition	Condition per condition	$n_{Ctr} = 9$, $n_{For} = 9$; 3 experiment, each contains 3 bands (endogenous, Eos4-geph, endogenous in Eos4-geph infected)	P<0.0001
Fig. 4B	Kruskal-Wallis test with Dunn's test as post hoc test	Mean intensity of each cluster in a cell	Cell by cell	$n_{Eos4\text{-}GephWTCtr} = 44$, $n_{Eos4\text{-}GephWT15} = 44$, $n_{Eos4\text{-}GephWT30} = 44$, $n_{Eos4\text{-}GephWT60} = 44$, $n_{Eos4\text{-}GephPKA\text{-}Ctr} = 42$, $n_{Eos4\text{-}GephPKA\text{-}15} = 43$, $n_{Eos4\text{-}GephPKA\text{-}30} = 44$, $n_{Eos4\text{-}GephPKA\text{-}60} = 45$	P<0.0001
Fig. 4C	1 way anova with Tukey's Multiple comparison test as post hoc test	Mean intensity of each cluster in a cell	Cell by cell	$n_{Ctr} = 60$, $n_{For} = 60$, $n_{For/H\text{-}89} = 60$	P<0.0001
Fig. 4E	1 way anova with Tukey's Multiple comparison test as post hoc test	Mean intensity of each cluster in a cell	Cell by cell	$n_{Ctr} = 90$, $n_{007} = 83$	P<0.0001
Fig. 4G	1 way anova with Tukey's Multiple comparison test as post hoc test	Mean intensity of each cluster in a cell	Cell by cell	$n_{Ctr} = 86$, $n_{For + Oka} = 84$	P<0.0001
Fig. 5B	Mann Whitney U test	Each value for each cluster	Cluster by cluster	$n_{Ctr} = 1237$, $n_{For} = 894$	Area P=0.1992; Detection P=0.8702; Detection/area P=0.0289
Fig. 5D	Mann Whitney U test	Each value for each cluster	Cluster by cluster	$n_{Ctr} = 8162$, $n_{For} = 7010$	Area P<0.0001; Detection P=0.0001; Detection/area P=0.0001
Fig. 6B	Kruskal-Wallis test with Dunn's test as post hoc test	D per each trajectory	Trajectory by trajectry	$n_{Ctr} = 730$, $n_{For} = 318$, $n_{007} = 384$	P<0.0001
Fig. 6C	Mann Whitney U test	D per each trajectory	Trajectory by trajectry	$n_{Ctr} = 1315$, $n_{For} = 1074$	P=0.0477
Fig. 6D	Mann Whitney U test	D per each trajectory	Trajectory by trajectry	a3L $n_{Ctr} = 1661$, $n_{For} = 1546$; a3K $n_{Ctr} = 1315$, $n_{For} = 1074$	a3L P<0.0001; a3K P=0.1304
Fig. S1B	Welch's t-test	Mean intensity of each cluster in a cell	Cell by cell	$n_{Ctr} = 80$, $n_{For} = 80$	P=0.2744
Fig. S1D Eos4 vs 7a	Kruskal-Wallis test with Dunn's test as post hoc test	Mean intensity of each cluster in a cell	Cell by cell	$n_{Eos4\text{-}GephWTCtr} = 44$, $n_{Eos4\text{-}GephWT15} = 44$, $n_{Eos4\text{-}GephWT30} = 44$, $n_{Eos4\text{-}GephWT60} = 44$	Eos P<0.0001, 7a P<0.0001
Fig. S1D GlyRa1	Kruskal-Wallis test	Mean intensity of each cluster in a cell	Cell by cell	$n_{Eos4\text{-}GephWTCtr} = 44$, $n_{Eos4\text{-}GephWT15} = 44$, $n_{Eos4\text{-}GephWT30} = 44$, $n_{Eos4\text{-}GephWT60} = 44$	P=0.0729
Fig. S1E Eos4 vs 7a	Kruskal-Wallis test with Dunn's test as post hoc test	Mean intensity of each cluster in a cell	Cell by cell	$n_{Eos4\text{-}GephPKA\text{-}Ctr} = 42$, $n_{Eos4\text{-}GephPKA\text{-}15} = 43$, $n_{Eos4\text{-}GephPKA\text{-}30} = 44$, $n_{Eos4\text{-}GephPKA\text{-}60} = 45$	Eos P=0.0085, 7a P<0.0001
Fig. S1E GlyRa1	Kruskal-Wallis test	Mean intensity of each cluster in a cell	Cell by cell	$n_{Eos4\text{-}GephPKA\text{-}Ctr} = 42$, $n_{Eos4\text{-}GephPKA\text{-}15} = 43$, $n_{Eos4\text{-}GephPKA\text{-}30} = 44$, $n_{Eos4\text{-}GephPKA\text{-}60} = 45$	P=0.2454
Fig. S3A	Welch's t-test	Mean value of each cluster in a image	Image by image	$n_{Ctr} = 32$, $n_{For} = 32$	Area P=0.6528; Detection P=0.1433; Detection/area P=0.7279
Fig. S3B	Welch's t-test	Mean value of each cluster in a image	Image by image	$n_{Ctr} = 70$, $n_{For} = 66$	Area P<0.0001; Detection P=0.0094; Detection/area P=0.0908
Fig. S4B	1 way anova with Tukey's Multiple comparison test as post hoc test	Mean intensity of each cluster in a cell	Cell by cell	$n_{Ctr} = 69$, $n_{For} = 60$	P<0.0001
Fig. S4C	1 way anova	Mean intensity of each cluster in a cell	Cell by cell	$n_{Ctr} = 51$, $n_{For} = 31$	P=0.6265
Fig. S4D	1 way anova with Tukey's Multiple comparison test as post hoc test	Mean intensity of each cluster in a cell	Cell by cell	$n_{Ctr} = 68$, $n_{For} = 69$	P=0.0121
Fig. S5B	1 way anova with Tukey's Multiple comparison test as post hoc test	Mean intensity of each cluster in a cell	Cell by cell	$n_{Ctr} = 146$, $n_{For} = 159$	P<0.0001
Fig. S5C	1 way anova with Tukey's Multiple comparison test as post hoc test	Mean intensity of each cluster in a cell	Cell by cell	$n_{Ctr} = 159$, $n_{For} = 146$	P<0.0001
Fig. S5D	1 way anova with Tukey's Multiple comparison test as post hoc test	Mean intensity of each cluster in a cell	Cell by cell	$n_{Ctr} = 164$, $n_{For} = 141$	P<0.0001

Table S2. Compilation of mean values and quartiles of the data in each graph (related to Figures 1-6).

Figure Number	mean	25%	median	75%
Fig. 1B GlyR Ctr	1	0.8419	0.9639	1.179
Fig. 1B GlyR For	0.9347	0.7528	0.8727	1.055
Fig. 1B $GABA_AR$ Ctr	1	0.8516	0.9954	1.128
Fig. 1B $GABA_AR$ For	0.8023	0.7088	0.8422	0.9403
Fig. 1B Geph 7a Ctr	1	0.8497	0.9512	1.182
Fig. 1B Geph 7a For	0.766	0.6166	0.7416	0.926
Fig. 1C GlyR/ 7a Ctr	1.176	0.8168	0.9931	1.205
Fig. 1C GlyR/ 7a For	1.564	0.9448	1.174	1.833
Fig. 1C $GABA_AR$/ 7a Ctr	1.09	0.8105	0.9997	1.253
Fig. 1C $GABA_AR$/ 7a For	1.178	0.789	1.044	1.431
Fig. 2B GlyR Ctr	1	0.5024	0.8338	1.323
Fig. 2B GlyR For	1.022	0.5111	0.8267	1.429
Fig. 2B Geph 7a Ctr	1	0.646	0.878	1.366
Fig. 2B Geph 7a For	0.5528	0.313	0.4519	0.6843
Fig. 2B Geph 3B11 Ctr	1	0.7992	0.9556	1.162
Fig. 2B Geph 3B11 For	0.9309	0.672	0.8848	1.092
Fig. 2D GlyR Ctr	1	0.7779	0.932	1.149
Fig. 2D GlyR For	1.014	0.6498	0.8532	1.133
Fig. 2D mRFP-Geph KI Ctr	1	0.769	0.9119	1.104
Fig. 2D mRFP-Geph KI For	0.884	0.6617	0.7812	1.077
Fig. 2E Ctr 2-3	0.8981	0.8032	0.8885	1.084
Fig. 2E Ctr 4-5	1.093	0.8971	1.022	1.075
Fig. 2E Ctr 6-7	1.021	0.924	1.063	1.119
Fig. 2E Ctr 8-9	1.123	1.065	1.123	1.187
Fig. 2E For 2-3	0.6681	0.4978	0.7131	0.8416
Fig. 2E For 4-5	0.7668	0.7246	0.8141	0.8588
Fig. 2E For 6-7	0.7985	0.7567	0.8121	0.9348
Fig. 2E For 8-9	0.8208	0.782	0.8463	0.9162
Fig. 3B Ctr	1.01	0.835	0.9861	1.196
Fig. 3B For	0.5517	0.4102	0.5597	0.6281
Fig. 4B Eos-$Geph^{wt}$ Ctr	1	0.5356	0.7982	0.9707
Fig. 4B Eos-$Geph^{wt}$ 15	0.5301	0.2085	0.4522	0.7173
Fig. 4B Eos-$Geph^{wt}$ 30	0.4431	0.1707	0.2994	0.5457
Fig. 4B Eos-$Geph^{wt}$ 60	0.5617	0.179	0.2714	0.5096
Fig. 4B Eos-$Geph^{PKA-}$ Ctr	1	0.6283	0.75	1.057
Fig. 4B Eos-$Geph^{PKA-}$ 15	0.3891	0.2098	0.3515	0.5174
Fig. 4B Eos-$Geph^{PKA-}$ 30	0.4935	0.1953	0.4527	0.5959
Fig. 4B Eos-$Geph^{PKA-}$ 60	0.4454	0.2135	0.3108	0.5395
Fig. 4C Ctr	1	0.7746	0.9813	1.194
Fig. 4C For	0.7968	0.6293	0.7605	0.9153
Fig. 4C For/H-89	0.8213	0.6386	0.766	0.9822
Fig. 4E GlyR Ctr	1	0.8024	0.9548	1.159
Fig. 4E GlyR 007	0.9447	0.7516	0.9273	1.075
Fig. 4E Geph 7a Ctr	1	0.7741	0.9735	1.216
Fig. 4E Geph 7a 007	0.8364	0.5808	0.8334	1.093
Fig. 4E $GABA_AR$ Ctr	1	0.7371	0.9739	1.192
Fig. 4E $GABA_AR$ 007	0.8368	0.623	0.8002	1.053
Fig. 4G Geph 3B11 For/H-89	1	0.8682	0.9816	1.146
Fig. 4G Geph 3B11 For/H-89/Oka	1.046	0.8617	0.9874	1.243
Fig. 4G Geph 7a For/H-89	1	0.7736	0.991	1.228
Fig. 4G Geph 7a For/H-89/Oka	1.171	0.9326	1.095	1.386
Fig. 5B area Ctr	0.05872	0.0253	0.0412	0.0765
Fig. 5B area For	0.05315	0.025	0.04205	0.0682
Fig. 5B detections Ctr	1316	324.5	657	1847
Fig. 5B detections For	1276	326.8	697	1808
Fig. 5B detections/area Ctr	1.976	1.233	1.666	2.419
Fig. 5B detections/area For	2.09	1.287	1.766	2.53
Fig. 5D area Ctr	0.02468	0.0114	0.01805	0.0302
Fig. 5D area For	0.01986	0.0098	0.0143	0.024
Fig. 5D detections Ctr	298.2	85	158	332
Fig. 5D detections For	259.6	76	127	270
Fig. 5D detections/area Ctr	1.103	0.672	0.8784	1.206
Fig. 5D detections/area For	1.136	0.7037	0.9143	1.245
Fig. 6B $GABA_Ag2$ Ctr	0.009697	0.0009782	0.002203	0.004024
Fig. 6B $GABA_Ag2$ For	0.01932	0.001768	0.00363	0.005805
Fig. 6B $GABA_Ag2$ 007	0.01281	0.001559	0.002816	0.005431
Fig. 6C GlyR a1 Ctr	0.0192	0.002985	0.008381	0.02186
Fig. 6C GlyR a1 For	0.01719	0.002333	0.007627	0.01899
Fig. 6C GlyR a3L Ctr	0.01035	0.001262	0.004172	0.01083
Fig. 6C GlyR a3L For	0.01452	0.001976	0.005843	0.0144
Fig. 6C GlyR a3K Ctr	0.0138	0.00214	0.006054	0.01631
Fig. 6C GlyR a3K For	0.01465	0.002427	0.006608	0.01631

Figure Number	mean	25%	median	75%
Fig. S1B Ctr	1	0.8488	0.9829	1.143
Fig. S1B For	1.043	0.86	0.9834	1.191
Fig. S1D Eos-$Geph^{wt}$ Ctr	1	0.7154	0.9307	1.337
Fig. S1D Eos-$Geph^{wt}$ 15	1.065	0.7931	1.105	1.348
Fig. S1D Eos-$Geph^{wt}$ 30	0.8914	0.5138	0.7487	1.121
Fig. S1D Eos-$Geph^{wt}$ 60	0.7714	0.4446	0.6718	0.936
Fig. S1D Geph 7a Ctr (WT)	1	0.7293	0.8516	1.108
Fig. S1D Geph 7a 15 (WT)	0.5939	0.2803	0.4969	0.7579
Fig. S1D Geph 7a 30 (WT)	0.3216	0.208	0.2847	0.4358
Fig. S1D Geph 7a 60 (WT)	0.4013	0.1308	0.2164	0.4347
Fig. S1D GlyRa1 Ctr (WT)	1	0.5136	0.7242	1.558
Fig. S1D GlyRa1 15 (WT)	0.9974	0.3667	0.8857	1.603
Fig. S1D GlyRa1 30 (WT)	0.8195	0.4041	0.76	1.1154
Fig. S1D GlyRa1 60 (WT)	0.7144	0.2483	0.5112	1.094
Fig. S1E Eos-$Geph^{PKA-}$ Ctr	1	0.6906	0.9692	1.199
Fig. S1E Eos-$Geph^{PKA-}$ 15	0.8216	0.5492	0.6972	1.027
Fig. S1E Eos-$Geph^{PKA-}$ 30	0.703	0.5016	0.6724	0.8509
Fig. S1E Eos-$Geph^{PKA-}$ 60	0.806	0.5733	0.7355	1.033
Fig. S1E Geph 7a Ctr (PKA-)	1	0.6045	0.8255	1.106
Fig. S1E Geph 7a 15 (PKA-)	0.3106	0.1491	0.3027	0.4631
Fig. S1E Geph 7a 30 (PKA-)	0.3413	0.1658	0.3339	0.5077
Fig. S1E Geph 7a 60 (PKA-)	0.3205	0.1754	0.2647	0.4188
Fig. S1E GlyRa1 Ctr (PKA-)	1	0.3421	0.9174	1.378
Fig. S1E GlyRa1 15 (PKA-)	0.8233	0.3503	0.6981	1.085
Fig. S1E GlyRa1 30 (PKA-)	0.81	0.1897	0.5456	1.367
Fig. S1E GlyRa1 60 (PKA-)	1.014	0.4568	0.7038	1.419
Fig. S3A area Ctr	0.05881	0.5547	0.0588	0.06628
Fig. S3A area For	0.05486	0.0469	0.05256	0.0609
Fig. S3A detections Ctr	1349	1111	1393	1004
Fig. S3A detections For	1307	1004	1223	1483
Fig. S3A detections/area Ctr	2.043	1.825	1.952	2.284
Fig. S3A detections/area For	2.078	1.753	1.998	2.36
Fig. S3B area Ctr	0.02445	0.0206	0.02341	0.02646
Fig. S3B area For	0.01905	0.01603	0.01877	0.02191
Fig. S3B detections Ctr	285.4	226.4	273	335
Fig. S3B detections For	247.4	181	227.2	299.7
Fig. S3B detections/area Ctr	1.073	0.945	1.022	1.183
Fig. S3B detections/area For	1.128	0.9916	1.1	1.248
Fig. S4B GlyRa3L Ctr	1	0.7556	0.9352	1.279
Fig. S4B GlyRa3L For	0.7865	0.5635	0.6781	0.9304
Fig. S4B Geph 7a Ctr (GlyRa3L)	1	0.7769	0.9543	1.1142
Fig. S4B Geph 7a For (GlyRa3L)	0.7829	0.5475	0.7371	1.008
Fig. S4C GlyRa1 Ctr	1	0.7018	0.887	1.252
Fig. S4C GlyRa1 For	1.004	0.6312	0.8648	1.147
Fig. S4C Geph 7a Ctr (GlyRa1)	1	0.697	1.026	1.236
Fig. S4C Geph 7a For (GlyRa1)	0.8878	0.6122	0.8515	1.187
Fig. S4D GlyRa3K Ctr	1	0.7385	0.9245	1.177
Fig. S4D GlyRa3K For	0.9077	0.6101	0.82	1.144
Fig. S4D Geph 7a Ctr (GlyRa3K)	1	0.7335	1.023	1.176
Fig. S4D Geph 7a For (GlyRa3K)	0.8136	0.5515	0.7047	1.059
Fig. S5B GlyRa3LWT Ctr	1	0.5736	0.8796	1.259
Fig. S5B GlyRa3LWT For	0.8289	0.5212	0.7639	1.104
Fig. S5B Geph 7a Ctr (WT)	1	0.7049	0.9454	1.286
Fig. S5B Geph 7a For (WT)	0.6713	0.4493	0.6567	0.8643
Fig. S5C GlyRa3LS346A Ctr	1	0.7274	0.9158	1.255
Fig. S5C GlyRa3LS346A For	0.9404	0.6599	0.9306	1.141
Fig. S5C Geph 7a Ctr (S346A)	1	0.6889	0.9261	1.238
Fig. S5C Geph 7a For (S346A)	0.7912	0.5303	0.7275	1.026
Fig. S5D GlyRa3LS346D Ctr	1	0.6272	0.9087	1.269
Fig. S5D GlyRa3LS346D For	1.107	0.6542	0.9287	1.506
Fig. S5D Geph 7a Ctr (S346D)	1	0.6945	0.9914	1.281
Fig. S5D Geph 7a For (S346D	0.7374	0.4985	0.7299	0.9673